

Observation of $\psi(4040)$ and $\psi(4160)$ decay into $\eta J/\psi$

X. L. Wang,^{11,53} Y. L. Han,¹¹ C. Z. Yuan,¹¹ C. P. Shen,²⁸ P. Wang,¹¹ I. Adachi,⁸ H. Aihara,⁴⁹ D. M. Asner,³⁷ V. Aulchenko,¹ T. Aushev,¹⁵ T. Aziz,⁴⁴ A. M. Bakich,⁴³ Y. Ban,³⁸ B. Bhuyan,⁹ G. Bonvicini,⁵⁴ A. Bozek,³² M. Bračko,^{25,16} J. Brodzicka,³² O. Brovchenko,¹⁸ T. E. Browder,⁷ P. Chen,³¹ B. G. Cheon,⁶ K. Cho,¹⁹ S.-K. Choi,⁵ Y. Choi,⁴² J. Dalseno,^{26,45} Z. Doležal,² Z. Drásal,² S. Eidelman,¹ S. Esen,³ H. Farhat,⁵⁴ J. E. Fast,³⁷ V. Gaur,⁴⁴ R. Gillard,⁵⁴ Y. M. Goh,⁶ B. Golob,^{23,16} H. Hayashii,²⁹ Y. Hoshi,⁴⁷ W.-S. Hou,³¹ H. J. Hyun,²¹ K. Inami,²⁸ A. Ishikawa,⁴⁸ M. Iwabuchi,⁵⁶ J. H. Kang,⁵⁶ P. Kapusta,³² H. J. Kim,²¹ H. O. Kim,²¹ J. B. Kim,²⁰ J. H. Kim,¹⁹ M. J. Kim,²¹ Y. J. Kim,¹⁹ K. Kinoshita,³ J. Klucar,¹⁶ B. R. Ko,²⁰ P. Kodyš,² R. T. Kouzes,³⁷ P. Krizán,^{23,16} P. Krokovny,¹ T. Kumita,⁵¹ J. S. Lange,⁴ S.-H. Lee,²⁰ J. Li,⁴¹ J. Libby,¹⁰ C. Liu,⁴⁰ Z. Q. Liu,¹¹ P. Lukin,¹ S. McOnie,⁴³ H. Miyata,³⁴ R. Mizuk,¹⁵ G. B. Mohanty,⁴⁴ A. Moll,^{26,45} N. Muramatsu,³⁹ R. Mussa,¹⁴ M. Nakao,⁸ S. Nishida,⁸ O. Nitoh,⁵² S. Ogawa,⁴⁶ T. Ohshima,²⁸ S. Okuno,¹⁷ S. L. Olsen,⁴¹ G. Pakhlova,¹⁵ H. Park,²¹ T. K. Pedlar,²⁴ R. Pestotnik,¹⁶ M. Petrič,¹⁶ L. E. Piilonen,⁵³ K. Prothmann,^{26,45} H. Sahoo,⁷ Y. Sakai,⁸ S. Sandilya,⁴⁴ D. Santel,³ T. Sanuki,⁴⁸ O. Schneider,²² C. Schwanda,¹² K. Senyo,⁵⁵ M. E. Sevier,²⁷ M. Shapkin,¹³ T.-A. Shibata,⁵⁰ J.-G. Shiu,³¹ A. Sibidanov,⁴³ F. Simon,^{26,45} P. Smerkol,¹⁶ Y.-S. Sohn,⁵⁶ E. Solovieva,¹⁵ S. Stanič,³⁵ M. Starič,¹⁶ T. Sumiyoshi,⁵¹ K. Tanida,⁴¹ G. Tatishvili,³⁷ Y. Teramoto,³⁶ K. Trabelsi,⁸ M. Uchida,⁵⁰ S. Uehara,⁸ Y. Unno,⁶ S. Uno,⁸ Y. Usov,¹ P. Vanhoefer,²⁶ G. Varner,⁷ C. H. Wang,³⁰ J. Wang,³⁸ M.-Z. Wang,³¹ K. M. Williams,⁵³ E. Won,²⁰ Y. Yamashita,³³ C. C. Zhang,¹¹ Z. P. Zhang,⁴⁰ V. Zhilich,¹ and A. Zupanc¹⁸

(The Belle Collaboration)

¹*Budker Institute of Nuclear Physics SB RAS and Novosibirsk State University, Novosibirsk 630090*

²*Faculty of Mathematics and Physics, Charles University, Prague*

³*University of Cincinnati, Cincinnati, Ohio 45221*

⁴*Justus-Liebig-Universität Gießen, Gießen*

⁵*Gyeongsang National University, Chinju*

⁶*Hanyang University, Seoul*

⁷*University of Hawaii, Honolulu, Hawaii 96822*

⁸*High Energy Accelerator Research Organization (KEK), Tsukuba*

⁹*Indian Institute of Technology Guwahati, Guwahati*

¹⁰*Indian Institute of Technology Madras, Madras*

¹¹*Institute of High Energy Physics, Chinese Academy of Sciences, Beijing*

¹²*Institute of High Energy Physics, Vienna*

¹³*Institute of High Energy Physics, Protvino*

¹⁴*INFN - Sezione di Torino, Torino*

¹⁵*Institute for Theoretical and Experimental Physics, Moscow*

¹⁶*J. Stefan Institute, Ljubljana*

¹⁷*Kanagawa University, Yokohama*

¹⁸*Institut für Experimentelle Kernphysik, Karlsruher Institut für Technologie, Karlsruhe*

¹⁹*Korea Institute of Science and Technology Information, Daejeon*

²⁰*Korea University, Seoul*

²¹*Kyungpook National University, Taegu*

²²*École Polytechnique Fédérale de Lausanne (EPFL), Lausanne*

²³*Faculty of Mathematics and Physics, University of Ljubljana, Ljubljana*

²⁴*Luther College, Decorah, Iowa 52101*

²⁵*University of Maribor, Maribor*

²⁶*Max-Planck-Institut für Physik, München*

²⁷*University of Melbourne, School of Physics, Victoria 3010*

²⁸*Graduate School of Science, Nagoya University, Nagoya*

²⁹*Nara Women's University, Nara*

³⁰*National United University, Miao Li*

³¹*Department of Physics, National Taiwan University, Taipei*

³²*H. Niewodniczanski Institute of Nuclear Physics, Krakow*

³³*Nippon Dental University, Niigata*

³⁴*Niigata University, Niigata*

³⁵*University of Nova Gorica, Nova Gorica*

³⁶*Osaka City University, Osaka*

³⁷*Pacific Northwest National Laboratory, Richland, Washington 99352*

³⁸*Peking University, Beijing*

³⁹*Research Center for Electron Photon Science, Tohoku University, Sendai*

⁴⁰*University of Science and Technology of China, Hefei*

⁴¹Seoul National University, Seoul

⁴²Sungkyunkwan University, Suwon

⁴³School of Physics, University of Sydney, NSW 2006

⁴⁴Tata Institute of Fundamental Research, Mumbai

⁴⁵Excellence Cluster Universe, Technische Universität München, Garching

⁴⁶Toho University, Funabashi

⁴⁷Tohoku Gakuin University, Tagajo

⁴⁸Tohoku University, Sendai

⁴⁹Department of Physics, University of Tokyo, Tokyo

⁵⁰Tokyo Institute of Technology, Tokyo

⁵¹Tokyo Metropolitan University, Tokyo

⁵²Tokyo University of Agriculture and Technology, Tokyo

⁵³CNP, Virginia Polytechnic Institute and State University, Blacksburg, Virginia 24061

⁵⁴Wayne State University, Detroit, Michigan 48202

⁵⁵Yamagata University, Yamagata

⁵⁶Yonsei University, Seoul

(Dated: October 14, 2018)

The cross section for $e^+e^- \rightarrow \eta J/\psi$ between $\sqrt{s} = 3.8$ GeV and 5.3 GeV is measured via initial state radiation using 980 fb^{-1} of data on and around the $\Upsilon(nS)$ ($n = 1, 2, 3, 4, 5$) resonances collected with the Belle detector at KEKB. Two resonant structures at the $\psi(4040)$ and $\psi(4160)$ are observed in the $\eta J/\psi$ invariant mass distribution. Fitting the mass spectrum with the coherent sum of two Breit-Wigner functions, one obtains $\mathcal{B}(\psi(4040) \rightarrow \eta J/\psi) \cdot \Gamma_{e^+e^-}^{\psi(4040)} = (4.8 \pm 0.9 \pm 1.4) \text{ eV}$ and $\mathcal{B}(\psi(4160) \rightarrow \eta J/\psi) \cdot \Gamma_{e^+e^-}^{\psi(4160)} = (4.0 \pm 0.8 \pm 1.4) \text{ eV}$ for one solution and $\mathcal{B}(\psi(4040) \rightarrow \eta J/\psi) \cdot \Gamma_{e^+e^-}^{\psi(4040)} = (11.2 \pm 1.3 \pm 1.9) \text{ eV}$ and $\mathcal{B}(\psi(4160) \rightarrow \eta J/\psi) \cdot \Gamma_{e^+e^-}^{\psi(4160)} = (13.8 \pm 1.3 \pm 2.0) \text{ eV}$ for the other solution, where the first errors are statistical and the second are systematic. This is the first measurement of this hadronic transition mode of these two states, and the partial widths to $\eta J/\psi$ are found to be about 1 MeV. There is no evidence for the $Y(4260)$, $Y(4360)$, $\psi(4415)$, or $Y(4660)$ in the $\eta J/\psi$ final state, and upper limits of their production rates in e^+e^- annihilation are determined.

PACS numbers: 14.40.Pq, 13.25.Gv, 13.66.Bc

Many charmonium and charmoniumlike states have been discovered at B -factories in the past decade. Some of these states are good candidates for conventional charmonium states, while others exhibit unusual properties consistent with expectations for exotic states such as a multi-quark state, molecule, hybrid, or the glueball [1]. In the vector sector, four exotic charmoniumlike structures, $Y(4008)$ and $Y(4260)$ in $e^+e^- \rightarrow \pi^+\pi^- J/\psi$ [2, 3] and $Y(4360)$ and $Y(4660)$ in $e^+e^- \rightarrow \pi^+\pi^- \psi(2S)$ [4, 5], have been reported via initial state radiation (ISR), in addition to the three known excited ψ states above $4.0 \text{ GeV}/c^2$: $\psi(4040)$, $\psi(4160)$, and $\psi(4415)$. It is unlikely that all seven of these states are charmonia, as the potential models predict only five vector states in this mass region [6]. The current understanding of these states is based on limited statistics, and the fact that some may be produced via mechanisms that are difficult to estimate theoretically, such as final state rescattering [1], makes the determination of which might be exotic even more challenging. In order to further the understanding of the nature of these states, it is important to investigate them using much larger data samples.

An important study is the investigation of hadronic transitions (either by an η or a pion pair) between these states and a lower charmonium state like the J/ψ . The CLEO collaboration measured $\sigma(e^+e^- \rightarrow \eta J/\psi) =$

$15^{+5}_{-4} \pm 8 \text{ pb}$ at $\sqrt{s} = 4120 - 4200 \text{ MeV}$ [7], and the BESIII collaboration reported $\sigma(e^+e^- \rightarrow \eta J/\psi) = (32.1 \pm 2.8) \text{ pb}$ at $\sqrt{s} = 4009 \text{ MeV}$ [8], which is in agreement with the theoretical calculation including contributions from the known ψ states and the virtual charmed meson loops [9]. However, the limited statistics of the CLEO analysis prevented the measurement of the line shape of $\eta J/\psi$. Thus, it is worthwhile to study the process $e^+e^- \rightarrow \eta J/\psi$ via ISR with the full Belle data sample to search for η transitions from these seven states to J/ψ . It is worth noting that the ψ states are identified in decays to charmed meson pairs but not in dipion transitions to lower ψ states, while the opposite is true of the Y states. There may also be surprises from transitions of unexpected states.

In this Letter, we report an investigation of the $e^+e^- \rightarrow \eta J/\psi$ process using ISR events observed with the Belle detector [10] at the KEKB asymmetric-energy e^+e^- collider [11]. Here, J/ψ is reconstructed in the $\ell^+\ell^-$ ($\ell = e, \mu$) final state and η in the $\gamma\gamma$ and $\pi^+\pi^-\pi^0$ final states. Due to the high background level from Bhabha scattering, the $J/\psi \rightarrow e^+e^-$ mode is not used in conjunction with the decay mode $\eta \rightarrow \gamma\gamma$. The integrated luminosity used in this analysis is 980 fb^{-1} . About 70% of the data were collected at the $\Upsilon(4S)$ resonance, and the rest were taken at other $\Upsilon(nS)$ ($n = 1, 2, 3$, or

5) states or center-of-mass (CM) energies a few tens of MeV lower than the $\Upsilon(4S)$ or the $\Upsilon(nS)$ peaks.

We use the PHOKHARA event generator [12] to simulate the process $e^+e^- \rightarrow \gamma_{\text{ISR}}\eta J/\psi$. In the generator, one or two ISR photons may be emitted before forming the resonance X , which then decays to $\eta J/\psi$, with $J/\psi \rightarrow e^+e^-$ or $\mu^+\mu^-$ and $\eta \rightarrow \pi^+\pi^-\pi^0$ or $\gamma\gamma$.

For a candidate event, we require two (four) good charged tracks with zero net charge for $\eta \rightarrow \gamma\gamma$ ($\eta \rightarrow \pi^+\pi^-\pi^0$). A good charged track has impact parameters with respect to the interaction point of $dr < 0.5$ cm in the r - ϕ plane and $|dz| < 5$ cm in the r - z plane. The transverse momentum of the leptons is required to be greater than 0.1 GeV/ c . For each charged track, information from different detector subsystems is combined to form a likelihood for each particle species (i), \mathcal{L}_i [13]. Tracks with $\mathcal{R}_K = \frac{\mathcal{L}_K}{\mathcal{L}_K + \mathcal{L}_\pi} < 0.4$ are identified as pions with an efficiency of about 95%, while 6% of kaons are misidentified as pions. Similar likelihood ratios are formed for electron and muon identification [14, 15]. For electrons from $J/\psi \rightarrow e^+e^-$, both tracks are required to have $\mathcal{R}_e > 0.1$. The bremsstrahlung photons detected in the electromagnetic calorimeter (ECL) within 0.05 radians of the original e^+ or e^- direction are included in the calculation of the e^+e^- (γ) invariant mass. For muons from $J/\psi \rightarrow \mu^+\mu^-$, one of the tracks is required to have $\mathcal{R}_\mu > 0.9$ and the other track should have associated hits in the K_L -and-muon detector (KLM) that agree with the extrapolated trajectory of a charged track provided by the drift chamber. The lepton ID efficiency is about 90% for $J/\psi \rightarrow e^+e^-$ and 87% for $J/\psi \rightarrow \mu^+\mu^-$.

The η is reconstructed from $\pi^+\pi^-\pi^0$ and $\gamma\gamma$ final states. To reconstruct $\eta \rightarrow \pi^+\pi^-\pi^0$, the π^0 is reconstructed from two photons. A photon candidate is an ECL cluster with energy $E(\gamma) > 25$ MeV that does not match any charged tracks. The mass resolution of π^0 is about 5.2 MeV/ c^2 from MC simulation. Considering the low-mass tail, the invariant mass of the photon pair is required to be between 110 MeV/ c^2 and 150 MeV/ c^2 for a π^0 candidate. $\pi^+\pi^-\pi^0$ combinations are formed and are subject to a mass-constrained kinematic fit. When there is more than one π^0 candidate, the combination with the smallest χ^2 from the mass-constrained fit is selected as the η candidate. Events with γ -conversions are removed by requiring $\mathcal{R}_e < 0.75$ for the $\pi^+\pi^-$ tracks from η decays. In the reconstruction of $\eta \rightarrow \gamma\gamma$ candidates, two photon candidates are required with energies in the laboratory frame satisfying $E(\gamma_l) > 0.15$ GeV and $E(\gamma_h) > 0.4$ GeV, where the subscript l (h) signifies the lower (higher) energy photon.

The scatter plots of dilepton invariant mass $M_{\ell^+\ell^-}$ versus η -candidate invariant mass $M_{\pi^+\pi^-\pi^0}$ or $\gamma_l\gamma_h$ invariant mass $M_{\gamma\gamma}$ are shown in Fig. 1 for events that survive these selection criteria. Here the invariant masses are calculated with the momenta before the mass constraints. A dilepton pair is considered as a

J/ψ candidate if $M_{\ell^+\ell^-}$ is within ± 45 MeV/ c^2 (the mass resolution being 15 MeV/ c^2) of the J/ψ nominal mass. The J/ψ mass sidebands are defined as $M_{\ell^+\ell^-} \in [3.172, 3.262]$ GeV/ c^2 or $M_{\ell^+\ell^-} \in [2.932, 3.022]$ GeV/ c^2 . A fit of the $M_{\pi^+\pi^-\pi^0}$ or $M_{\gamma\gamma}$ distribution with a Gaussian plus a second-order polynomial yields a mass resolution of 4.3 MeV/ c^2 for the $\eta \rightarrow \pi^+\pi^-\pi^0$ mode and 11.1 MeV/ c^2 for the $\eta \rightarrow \gamma\gamma$ mode. We define the η signal region as $M_{\pi^+\pi^-\pi^0} \in [0.5343, 0.5613]$ GeV/ c^2 and $M_{\gamma\gamma} \in [0.5, 0.6]$ GeV/ c^2 and the η mass sideband regions as $M_{\pi^+\pi^-\pi^0} \in [0.5748, 0.6018]$ GeV/ c^2 or $M_{\pi^+\pi^-\pi^0} \in [0.4938, 0.5208]$ GeV/ c^2 , and $M_{\gamma\gamma} \in [0.35, 0.45]$ GeV/ c^2 or $M_{\gamma\gamma} \in [0.65, 0.75]$ GeV/ c^2 . The central (surrounding) rectangles of Fig. 1 show the $\eta J/\psi$ signal (sideband) regions. With $S1$ ($S2$) representing the sum of the events in the four sideband boxes nearest (diagonal) to the signal box, the normalization of the sidebands is $S = 0.5 \times S1 - 0.25 \times S2$.

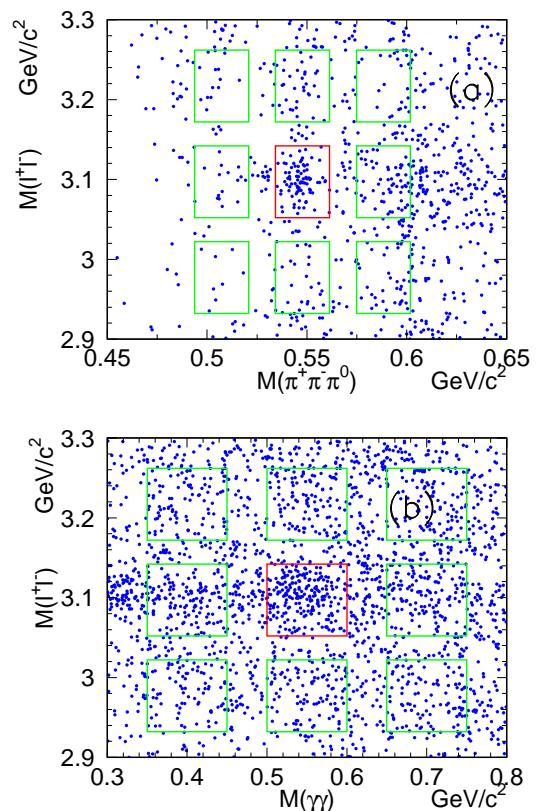


FIG. 1: Invariant mass distributions of (a) $\ell^+\ell^-$ vs. $\pi^+\pi^-\pi^0$ and (b) $\ell^+\ell^-$ vs. $\gamma\gamma$ for selected $\pi^+\pi^-\pi^0\ell^+\ell^-$ or $\gamma\gamma\ell^+\ell^-$ candidates with invariant mass between 3.8 GeV/ c^2 and 5.3 GeV/ c^2 . The box in the center of each plot shows the $\eta J/\psi$ signal region while the surrounding boxes show the sideband regions.

The detection of the ISR photon is not required; instead, we require $-1 (\text{GeV}/c^2)^2 < M_{\text{rec}}^2 < 2.0 (\text{GeV}/c^2)^2$, where M_{rec}^2 is the square of the mass re-

coiling against the $\eta J/\psi$ system. In calculating M_{rec}^2 , the momenta of the J/ψ and η after the kinematic fit are used to improve the resolution of M_{rec}^2 . The fit constrains signal candidates to the η and J/ψ masses, while events having η or J/ψ candidate masses lying in sideband regions are fitted with masses constrained to the center of the sideband region.

Figure 2 shows the $\eta J/\psi$ invariant mass ($M_{\eta J/\psi}$ [16]) for selected candidate events, together with background estimated from the scaled η or J/ψ mass sidebands. Two distinct peaks are evident in Fig. 2, one at 4.0 GeV/c^2 and the other at 4.2 GeV/c^2 , in addition to the dominant $\psi(2S)$ signal. The cross section of $e^+e^- \rightarrow \gamma_{\text{ISR}}\psi(2S)$ in the full Belle data sample is measured to be 13.9 ± 1.4 (stat.) pb using the 186 ± 17 $\eta \rightarrow \pi^+\pi^-\pi^0$ events and 14.0 ± 0.8 (stat.) pb using the 470 ± 25 $\eta \rightarrow \gamma\gamma$ events, in good agreement with the production cross section of 14.7 pb calculated by using the world average values of the mass, width, and partial width to e^+e^- of $\psi(2S)$ [17], and the e^+e^- CM energies correspond to the Belle data samples. Agreement between the $J/\psi \rightarrow e^+e^-$ and $J/\psi \rightarrow \mu^+\mu^-$ modes is also observed. The visible energy (E_{vis}) and polar angle distributions of the $\eta J/\psi$ system in the e^+e^- CM frame for the events with $M_{\eta J/\psi} \in [3.8, 5.3]$ GeV/c^2 agree well with the MC simulation, confirming that the signal events are produced via ISR. Here, E_{vis} is the total energy of all final state photons and charged particles. Charged particle energies are calculated from track momenta assuming the tracks to be pions.

An unbinned maximum likelihood fit is performed to the mass spectra $M_{\eta J/\psi} \in [3.8, 4.8]$ GeV/c^2 from the signal candidate events and η and J/ψ sideband events simultaneously, as shown in Fig. 3. The fit to the signal events includes two coherent P -wave Breit-Wigner functions, BW_1 for $\psi(4040)$ and BW_2 for $\psi(4160)$, assuming that only two resonances contribute to the $\eta J/\psi$ final states, and an incoherent second-order polynomial background; the fit to the sideband events includes the same background function only. The width of each resonance is assumed to be constant, and an overall two-body phase-space factor is applied in the partial width to $\eta J/\psi$. The signal amplitude is $M = BW_1 + e^{i\phi} \cdot BW_2$, where ϕ is the relative phase between the two resonances. In the fit, the BW functions are convolved with the effective luminosity [18] and $M_{\eta J/\psi}$ -dependent efficiency, which increases from 4% at $M_{\eta J/\psi} = 4.0$ GeV/c^2 to 7% at $M_{\eta J/\psi} = 4.5$ GeV/c^2 . The effect of mass resolution, which is determined from MC simulation to be 5 – 11 MeV/c^2 over the resonant mass region, is small compared with the widths of the observed structures, and therefore is neglected. A fit performed with floating masses and widths for the two structures yields a mass of (4012 ± 5) MeV/c^2 and width of (54 ± 13) MeV for the first, and a mass of (4157 ± 10) MeV/c^2 and width of (84 ± 20) MeV for the second. Their masses and widths

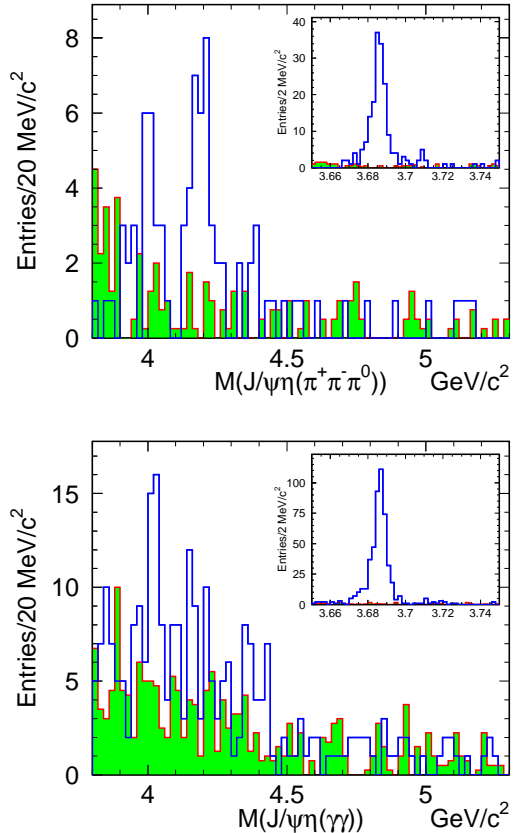


FIG. 2: The invariant mass distribution of the $\eta J/\psi$ candidates. The top row shows the $\eta \rightarrow \pi^+\pi^-\pi^0$ mode and the bottom row shows the $\eta \rightarrow \gamma\gamma$ mode. The open histograms are from the η and J/ψ signal region, while the shaded ones are from their sideband regions after the proper normalization. The insets show the distributions around the $\psi(2S)$ mass region.

are in agreement with those of the $\psi(4040)$ and $\psi(4160)$, and thus they are referred to hereafter as the $\psi(4040)$ and $\psi(4160)$. In the fit below, the masses and widths of these two resonances are fixed to their world average values [17] as the statistics are low here.

Figure 3 and Table I [19] show the fit results. There are two solutions with equally good fit quality. To determine the goodness of the fit, we bin the data (events in both signal and sideband regions) so that the expected number of events in a bin is at least seven and then calculate a χ^2/ndf of 71.4/46, corresponding to a confidence level (C.L.) of 0.9%, where ndf is the number of degrees of freedom. The significance of each resonance is estimated by comparing the likelihood of fits with and without that resonance included. We obtain a statistical significance of 6.5σ for $\psi(4040)$ and 7.6σ for $\psi(4160)$. Varying the masses and widths of resonances by 1σ , the fit range by 200 MeV/c^2 , and the order of the background polynomial by one, we obtain a minimum statistical significance of

6.0 σ for $\psi(4040)$ and 6.5 σ for $\psi(4160)$.

Taking $\Gamma_{e^+e^-}^{\psi(4040)} = (0.86 \pm 0.07)$ keV from PDG [17], one obtains $\mathcal{B}(\psi(4040) \rightarrow \eta J/\psi) = (0.56 \pm 0.10 \pm 0.17)\%$ or $\mathcal{B}(\psi(4040) \rightarrow \eta J/\psi) = (1.30 \pm 0.15 \pm 0.24)\%$; while using the PDG average value $\Gamma_{e^+e^-}^{\psi(4160)} = (0.83 \pm 0.07)$ keV [17], one gets $\mathcal{B}(\psi(4160) \rightarrow \eta J/\psi) = (0.48 \pm 0.10 \pm 0.17)\%$ or $(1.66 \pm 0.16 \pm 0.28)\%$. In each case, the first error is statistical and the second is systematic. These indicate the transition rates of these states to $\eta J/\psi$ are large, being of order 1 MeV.

Possible contributions from other excited charmonium(like) states are examined. There is a cluster of events near the $M_{\eta J/\psi} = 4.36$ GeV/ c^2 . Assuming it is the $Y(4360)$, the significance is 1.1 σ in a fit with the masses and widths of the $\psi(4040)$ and $\psi(4160)$ fixed to their world average values [17], or 2.9 σ if the masses and widths of $\psi(4040)$ and $\psi(4160)$ are free. Besides the $Y(4360)$, the $Y(4260)$, $\psi(4415)$ and $Y(4660)$ are in [3.8, 5.3] GeV/ c^2 mass region. Fits that include each one of them and the masses and widths of $\psi(4040)$ and $\psi(4160)$ fixed to their world average values [17] are performed to determine the upper limits of $\mathcal{B} \cdot \Gamma_{e^+e^-}$. The systematic errors that will be described later in the text together with those from the uncertainties of the $\psi(4040)$ and $\psi(4160)$ resonant parameters are considered in the upper limit determination. In order to be conservative, the efficiencies have been lowered by a factor of $1 - \sigma_{sys}$ in the calculation. We obtain the upper limits on $\mathcal{B}(X \rightarrow \eta J/\psi) \cdot \Gamma_{e^+e^-}^X$ for $X = Y(4260)$, $Y(4360)$, $\psi(4415)$ and $Y(4660)$ are 14.2 eV, 6.8 eV, 3.6 eV and 0.94 eV at 90% C.L., respectively.

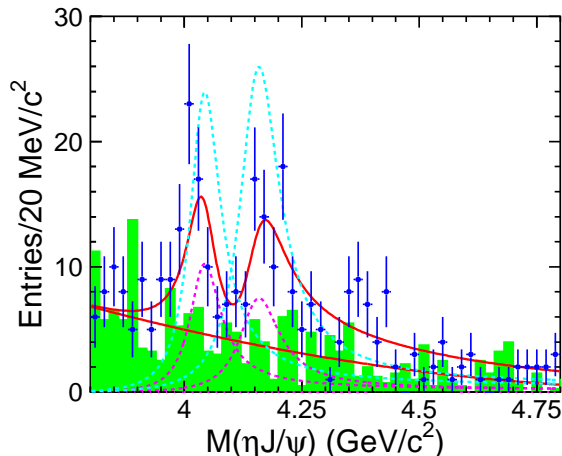


FIG. 3: The $\eta J/\psi$ invariant mass distribution and the fit results. The points with error bars show the data while the shaded histogram is the normalized η and J/ψ background from the sidebands. The curves show the best fit on signal candidate events and sideband events simultaneously and the contribution from each Breit-Wigner component. The interference between the two resonances is not shown. The dashed curves at each peak show the two solutions (see text).

TABLE I: Results of the fits to the $\eta J/\psi$ invariant mass spectrum. The first errors are statistical and the second are systematic. M , Γ , and $\mathcal{B} \cdot \Gamma_{e^+e^-}^{\psi}$ are the mass (in MeV/ c^2), total width (in MeV), product of the branching fraction of $\psi \rightarrow \eta J/\psi$ and the $\psi \rightarrow e^+e^-$ partial width (in eV), respectively. ϕ is the relative phase between the two resonances (in degrees).

Parameters	Solution I	Solution II
$M_{\psi(4040)}$	4039 (fixed)	
$\Gamma_{\psi(4040)}$	80 (fixed)	
$\mathcal{B} \cdot \Gamma_{e^+e^-}^{\psi(4040)}$	$4.8 \pm 0.9 \pm 1.4$	$11.2 \pm 1.3 \pm 1.9$
$M_{\psi(4160)}$	4153 (fixed)	
$\Gamma_{\psi(4160)}$	103 (fixed)	
$\mathcal{B} \cdot \Gamma_{e^+e^-}^{\psi(4040)}$	$4.0 \pm 0.8 \pm 1.4$	$13.8 \pm 1.3 \pm 2.0$
ϕ	$336 \pm 12 \pm 14$	$251 \pm 4 \pm 7$

To estimate the errors in $\mathcal{B} \cdot \Gamma_{e^+e^-}$, the uncertainties from the choice of parametrization of the resonances (especially introducing the mass dependence for the widths), the masses and widths of resonances [17], the fit range, the background shape and the possible contributions from $\psi(2S)$ or $\psi(4415)$ are considered. The total errors are 35.0% and 14.8% for solutions I and II, respectively. The particle ID uncertainty is 5.5%; the uncertainty in the tracking efficiency is 0.35% per track and is additive; the uncertainty in the photon reconstruction is 2% per photon. The uncertainties in the J/ψ mass, η mass, and M_{rec}^2 requirements are measured with the control sample $e^+e^- \rightarrow \psi(2S) \rightarrow \eta J/\psi$. The efficiencies of the requirements on the data are obtained from the fits of the corresponding distributions. The MC efficiency is found to be higher than in data by $(2.3 \pm 2.6)\%$ for the $\pi^+\pi^-\pi^0$ mode and $(0.1 \pm 1.6)\%$ for the $\gamma\gamma$ mode. A correction factor 1.023 is applied to the $\pi^+\pi^-\pi^0$ final state, and 2.6% is conservatively taken as the associated systematic error of the sum for $\pi^+\pi^-\pi^0$ and $\gamma\gamma$ modes.

Belle measures luminosity with 1.4% precision while the uncertainty of the generator PHOKHARA is less than 1% [12]. The trigger efficiency for the events surviving the selection criteria is around 91% with an uncertainty smaller than 2%. The uncertainties in the intermediate decay branching fractions taken from Ref. [17] contribute a systematic error of less than 1.6%. The statistical error in the MC determination of the efficiency is 0.2%.

Assuming all the sources are independent and adding them in quadrature, we obtain total systematic errors in $\mathcal{B} \cdot \Gamma_{e^+e^-}$ of 36% for Solution I and 17% for Solution II for both $\psi(4040)$ and $\psi(4160)$.

The cross section for $e^+e^- \rightarrow \eta J/\psi$ for each $\eta J/\psi$ mass bin is calculated according to

$$\sigma_i = \frac{n_i^{\text{obs}} - n_i^{\text{bkg}}}{\mathcal{L}_i \times \sum_j \varepsilon_{ij} \mathcal{B}_j},$$

where j is the j -th mode of $\eta J/\psi$ decays ($j = \pi^+\pi^-\pi^0 e^+e^-$, $\pi^+\pi^-\pi^0 \mu^+\mu^-$, and $\gamma\gamma\mu^+\mu^-$); n_i^{obs} , n_i^{bkg} , ε_{ij} , \mathcal{L}_i , and \mathcal{B}_j are number of events observed in data, number of background events estimated from sidebands, detection efficiency of the j -th mode, effective luminosity in the i -th $\eta J/\psi$ mass bin, and the branching fraction of $\eta J/\psi$ decays into the j -th mode [17], respectively. The resulting cross sections in the full solid angle are shown in Fig. 4, where the error bars include the statistical uncertainties in the signal and the background subtraction. The systematic error for the cross section measurement, which includes all the sources that have been described other than those arising from the details of the fit to the mass spectrum, is 8.0% and common to all the data points. The cross sections of $e^+e^- \rightarrow \eta J/\psi$ are around 70 pb and 50 pb at the $\psi(4040)$ and $\psi(4160)$ peaks, respectively, to be compared with around 20 pb and 10 pb measured in $e^+e^- \rightarrow \pi^+\pi^- J/\psi$ [2].

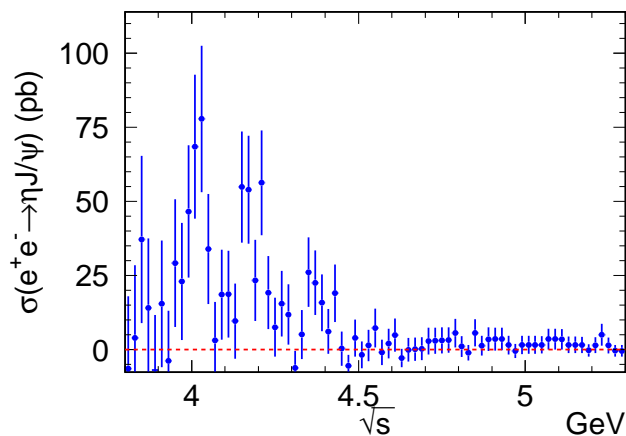


FIG. 4: The measured $e^+e^- \rightarrow \eta J/\psi$ cross section for $\sqrt{s} = 3.8$ GeV to 5.3 GeV. The errors are the summed statistical errors of the numbers of signal and background events. A systematic error of 8.0% common to all the data points are not shown.

In summary, the $e^+e^- \rightarrow \eta J/\psi$ cross section is measured from 3.8 GeV up to 5.3 GeV for the first time. Two distinct resonant structures, the $\psi(4040)$ and $\psi(4160)$, are observed. This is the first time that the $\psi(4040)$ and $\psi(4160)$ have been observed to decay to final states not involving charm meson pairs. The products of the branching fraction to $\eta J/\psi$ and the e^+e^- partial width are determined to be $\mathcal{B}(\psi(4040) \rightarrow \eta J/\psi) \cdot \Gamma_{e^+e^-}^{\psi(4040)} = (4.8 \pm 0.9 \pm 1.4)$ eV and $\mathcal{B}(\psi(4160) \rightarrow \eta J/\psi) \cdot \Gamma_{e^+e^-}^{\psi(4160)} = (4.0 \pm 0.8 \pm 1.4)$ eV for one solution; or $\mathcal{B}(\psi(4040) \rightarrow \eta J/\psi) \cdot \Gamma_{e^+e^-}^{\psi(4040)} = (11.2 \pm 1.3 \pm 1.9)$ eV and $\mathcal{B}(\psi(4160) \rightarrow \eta J/\psi) \cdot \Gamma_{e^+e^-}^{\psi(4160)} = (13.8 \pm 1.3 \pm 2.0)$ eV for the other solution. These transition rates correspond to about 1 MeV partial widths to $\eta J/\psi$ for these two states. We find no evidence for the $Y(4260)$, $Y(4360)$, $\psi(4415)$ or

$Y(4660)$ in the $\eta J/\psi$ final states, and upper limits of their production rates in e^+e^- annihilation are determined. The present measurement reveals clear peaks due to the $\psi(4040)$ and $\psi(4160)$ decays observed in experimental data that are absent in the prediction in Ref. [9], although the theoretical calculation with carefully chosen parameters agrees with the measured cross sections of $e^+e^- \rightarrow \eta J/\psi$.

We thank the KEKB group for excellent operation of the accelerator; the KEK cryogenics group for efficient solenoid operations; and the KEK computer group, the NII, and PNNL/EMSL for valuable computing and SINET4 network support. We acknowledge support from MEXT, JSPS and Nagoya's TLPRC (Japan); ARC and DIISR (Australia); NSFC (China); MSMT (Czechia); DST (India); INFN (Italy); MEST, NRF, GSDC of KISTI, and WCU (Korea); MNiSW (Poland); MES and RFAAE (Russia); ARRS (Slovenia); SNSF (Switzerland); NSC and MOE (Taiwan); and DOE and NSF (USA).

-
- [1] For a recent review, see N. Brambilla *et al.*, *Eur. Phys. J. C* **71**, 1534 (2011).
 - [2] C. Z. Yuan *et al.* (Belle Collaboration), *Phys. Rev. Lett.* **99**, 182004 (2007).
 - [3] B. Aubert *et al.* (BaBar Collaboration), *Phys. Rev. Lett.* **95**, 142001 (2005); J. P. Lees *et al.* (BaBar Collaboration), *Phys. Rev. D* **86**, 051102 (2012).
 - [4] X. L. Wang *et al.* (Belle Collaboration), *Phys. Rev. Lett.* **99**, 142002 (2007).
 - [5] B. Aubert *et al.* (BaBar Collaboration), *Phys. Rev. Lett.* **98**, 212001 (2007).
 - [6] S. Godfrey and N. Isgur, *Phys. Rev. D* **32**, 189 (1985); T. Barnes, S. Godfrey and E. S. Swanson, *Phys. Rev. D* **72**, 054026 (2005); G. J. Ding, J. J. Zhu and M. L. Yan, *Phys. Rev. D* **77**, 014033 (2008).
 - [7] T. E. Coan *et al.* (CLEO Collaboration), *Phys. Rev. Lett.* **96**, 162003 (2006).
 - [8] M. Ablikim *et al.* (BESIII Collaboration), *Phys. Rev. D* **86**, 071101 (2012).
 - [9] Q. Wang, X. H. Liu and Q. Zhao, *Phys. Rev. D* **84**, 014007 (2011).
 - [10] A. Abashian *et al.* (Belle Collaboration), *Nucl. Instrum. Methods A* **479**, 117 (2002).
 - [11] S. Kurokawa and E. Kikutani, *Nucl. Instrum. Methods A* **499**, 1 (2003) and other papers included in this volume.
 - [12] G. Rodrigo *et al.*, *Eur. Phys. J. C* **24**, 71 (2002). For a review on the generator, see: S. Actis *et al.*, *Eur. Phys. J. C* **66**, 585 (2010).
 - [13] E. Nakano, *Nucl. Instrum. Methods A* **494**, 402 (2002).
 - [14] K. Hanagaki *et al.*, *Nucl. Instrum. Methods A* **485**, 490 (2002).
 - [15] A. Abashian *et al.*, *Nucl. Instrum. Methods A* **491**, 69 (2002).
 - [16] $M_{\eta J/\psi} = M_{\pi^+\pi^-\pi^0\ell^+\ell^-} - M_{\pi^+\pi^-\pi^0} - M_{\ell^+\ell^-} + m_\eta + m_{J/\psi}$ for the $\eta \rightarrow \pi^+\pi^-\pi^0$ mode and $M_{\eta J/\psi} = M_{\gamma\gamma\ell^+\ell^-} - M_{\gamma\gamma} - M_{\ell^+\ell^-} + m_\eta + m_{J/\psi}$ for the $\eta \rightarrow \gamma\gamma$ mode, where

m_η and $m_{J/\psi}$ are the nominal η and J/ψ masses, respectively.

- [17] J. Beringer *et al.* (Particle Data Group), Phys. Rev. D **86**, 010001 (2012).
- [18] E. A. Kuraev and V. S. Fadin, Sov. J. Nucl. Phys. **41**, 466 (1985) [Yad. Fiz. **41**, 733 (1985)].
- [19] Fitting the $M_{\eta J/\psi}$ spectrum with the product $\mathcal{B}(\psi \rightarrow \eta J/\psi) \cdot \mathcal{B}(\psi \rightarrow e^+ e^-)$ as a parameter, and the masses

and widths of $\psi(4040)$ and $\psi(4160)$ fixed to world average values [17], we obtain $\mathcal{B}(\psi \rightarrow \eta J/\psi) \cdot \mathcal{B}(\psi \rightarrow e^+ e^-) = (5.1 \pm 1.4 \pm 1.4) \times 10^{-8}$ and $(2.8 \pm 0.9 \pm 0.9) \times 10^{-8}$ for the $\psi(4040)$ and $\psi(4160)$, respectively, for solution I; and $\mathcal{B}(\psi \rightarrow \eta J/\psi) \cdot \mathcal{B}(\psi \rightarrow e^+ e^-) = (12.8 \pm 2.1 \pm 1.7) \times 10^{-8}$ and $(12.8 \pm 1.7 \pm 1.9) \times 10^{-8}$ for the $\psi(4040)$ and $\psi(4160)$, respectively, for solution II.